Destructive Tests of Full-Size Rocket Motor Cases and Their Application to Lightweight Design

BENJAMIN C. F. WEI*
Curtiss-Wright Corporation, Wood-Ridge, N. J.

This paper describes experimental stress investigations of burst-tests under internal pressure of three full-size rocket motor cases made of Ladish D6AC steel. Two full-size cases made of 18% Ni maraging steel were also burst-tested for strength evaluation. Fifteen subscale vessels were also tested to destruction. Electric strain gages (SR-4) were used in all tests. Strain data in the plastic region were reduced by a digital computer. The results indicated that 1) a biaxial ultimate strength equal to 343 ksi has been achieved in 18% Ni maraging steel rocket motor cases; 2) within the range of radius-to-thickness ratios between 40 and 300, the subscale vessels behave essentially in the same way as the full-size cases with respect to the biaxial gains and the total elongation of the vessel at failure; 3) in a 2:1 stress field, the experimental biaxial gains in the elastic range vary from 15.5 to 16.5%, which are in close agreement with values predicted by Huber-Hencky-Von Mises theory of constant energy of distortion; 4) the experimental biaxial gains in the cylinder at fracture are in the range of 13 to 16%; and 5) the total elongations in the cylindrical vessels at failure are approximately one-fifth of those obtained from the uniaxial specimens.

Introduction

THE increasing emphasis on lightweight design of rocket motor cases to better the over-all performance of a missile system has introduced new design criteria, based on which the margin of safety of the shell structure is obtained with reference to the biaxial ultimate strength of the material. This biaxial ultimate strength can generally be established experimentally by burst-testing of subscale cylindrical vessels. However, because of the differences in the radius-to-thickness ratios, the authenticity of applying subscale data to full-scale missile case design has often been questioned by designers.

Strength theories, such as the Huber-Hencky-Von Mises distortion energy theorem, offer theoretical justifications for using major true stress in a biaxial stress field such as that which occurs in the cylindrical portion of the rocket motor case. However, the basic derivation of the theory is based on Hooke's law,[1] thus limiting the theoretical application up to yield point of the material.

By far the best and most reliable biaxial strength data are obtained from burst-testings of full-scale flightweight vessels. For large diameter rocket motor cases, such burst tests involve enormously high costs. However, the high costs have been justified by the reliable data generated, and by weight reductions of the missile cases through subsequent improved design. As a result, current practice in qualifying a new design of a rocket motor case generally requires bursting of one or more full-size flightweight vessels. These burst tests are in addition to the proof tests conducted in the early stage to check out the theoretical stresses under proof pressure.[2, 3]

This paper presents the results of burst-tests under internal pressure of three full-size 65-in.-diam rocket motor cases. These cases are made of Ladish D6AC steel representing the present "state-of-the-art" steel for large boosters. In addition, two full-size rocket motor cases, one 40 in. and the other 65 in. in diameter, fabricated from the ultra-high strength 18% Ni maraging steel were also burst-tested for material and strength evaluation.

Presented as Preprint 64-445 at the 1st AIAA Annual Meeting, Washington, D. C., June 29–July 2, 1964; revision received November 5, 1964. The author wishes to thank J. Sohn, Chief Metallurgist, Wright Aeronautical Division, for his valuable suggestions and critical review of this paper.

* Chief Project Engineer, Rocket Structures Group, Wright Aeronautical Division. Member AIAA.

The burst-test data of 12 14-in.-diam D6AC subscale vessels, nine tested at room temperature and three at 350°F, are also included. Similar data for three 18% Ni 6-in.-diam subscale vessels are also given. These subscale data are included to substantiate the findings of the full-size tests and to investigate the size effects on the strengths of the rocket motor cases.

Description of Tests

Selection of Gages and Their Locations

The SR-4 electric strain gages in the subscale vessels are generally located at outer surface and axially at midlength of the cylinder. The gages are repeated every 90° circumferentially to detect any variation of strain readings due to out-of-roundness of the cylinder. The design of a typical subscale vessel is shown in Fig. 1. The design incorporates reusable end cover plates.

For the full-size vessels, the gages are also located at middle sections of the cylinders. In order to locate the points of maximum strain under applied pressure, additional gages are placed at local thin areas of the cylinder. The dimensional inspection for thin areas is accomplished by laying out axial and circumferential grids over the complete periphery of the cylinder. The minimum wall thickness within each grid square is determined by scanning the grid with an ultrasonic Vidigage, which measures wall thicknesses to within ±0.001 in. In addition to the strain gages, extensometers are lo-

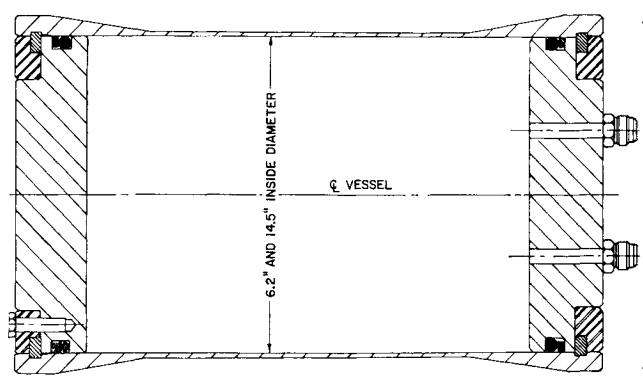

Fig. 1 Typical subscale vessel design.

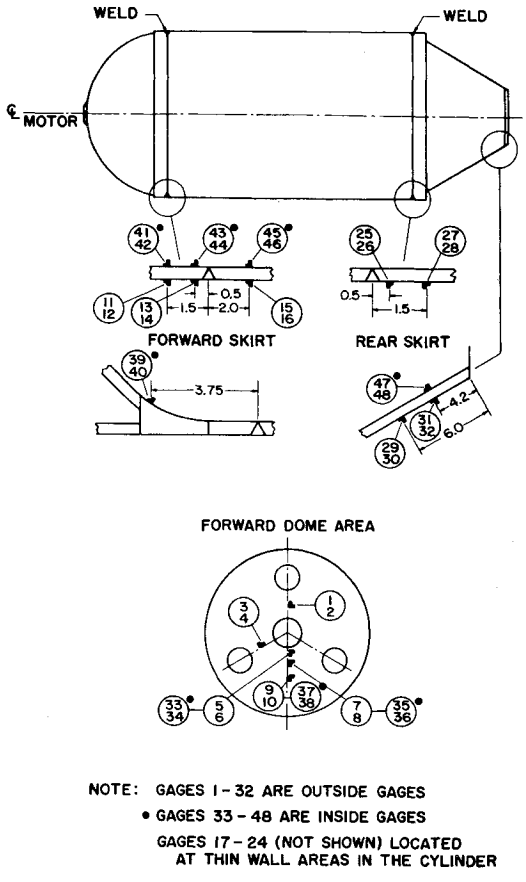

Fig. 2 Typical instrumentation of a 40-in.-diam, 18% Ni rocket motor case.

cated circumferentially along the periphery of the rocket case to measure the circumferential growths of the cylinder under pressure. Typical instrumentation layouts for the full-size 18% Ni and D6AC cases are shown in Figs. 2 and 3, respectively.

For room-temperature burst tests, the Baldwin-Lima-Hamilton (BLH) postyield PA-7 gages have proven reliable over a large number of experiments. Using a nonconducting oil as a testing medium, PA-7 gages also gave satisfactory results for interior applications. For the series of tests conducted, PA-7 gages have measured strains up to 4.9%. When the biaxial total strain of the material is expected to be 2.5% or less, the BLH FAB-50 gages will also yield satisfactory results.

The performance of gages in measuring large strains at elevated temperature (350°F) has not been fully established. As a result of experimental investigations, a maximum strain of 3.3% has been obtained with a BLH EBF-7S gage in combination with Epoxy 400 cement. The next best combination that recorded a maximum strain of 2.6% at 350°F consists of a BLH FAB-50 gage with the same cement.

The continuous recording of strains during the burst test is accomplished remotely by an oscillograph. The oscillograph provides a simultaneous and permanent record of time, pressure, and strains from the beginning to the end of a burst test. All of these entities are recorded as time-displacement curves on different channels and can be readily converted to finite strains, pressures, or deflections by using proper calibrations.

The pressure is read visually on a calibrated Heise gage. The pressure signals are also obtained from two calibrated transducers, one of which is continuously recorded on an oscillograph channel as previously described and the other on a Brown Recorder giving a direct pressure-time trace. Duplication of instrumentation in using different sources of signals and recording equipment provides a necessary check on the accuracy of results and assures reliable and useful data even though certain parts of the instrumentation may unexpectedly malfunction in the course of the test.

Test Procedure for Full-Size Rocket Motor Cases

After the case is instrumented, it is erected in vertical position on the test rig. The internal gage leads are brought out through the pyrogen boss substituting cover. A thrust piston and adapter are assembled to the aft nozzle flange of the case by means of which a simulated firing load is transmitted to the forward thrust skirt through the supporting gantry. The thrust piston assembly is used to eliminate unnecessary bending loads on the nozzle flange and to achieve a realistic thrust load on the forward skirt.

After the installation of the case in the gantry, it is filled with light spindle oil. The case is purged of any inside air and then checked for leaks by pressurizing to approximately one quarter of the estimated burst pressure. When the temperature of the testing medium is stabilized, the forementioned pressure is cycled three times to condition the strain gages. Elaborate checkings of the gage operation are made at this relatively low-pressure level until all of instrumentations are found to operate satisfactorily. The burst tests will then proceed at this point.

To simulate the actual firing of the rocket boosters, the bursting of the case from the proof pressure level is to be accomplished within a specific length of time. Longitudinal views of typical burst vessels are shown in Figs. 4–6.

Data Reduction

Stresses in the Plastic Region

For the hydroburst tests, the stresses in the inelastic range are determined from the postyield strain gages. The analytical method used is summarized below.[4]

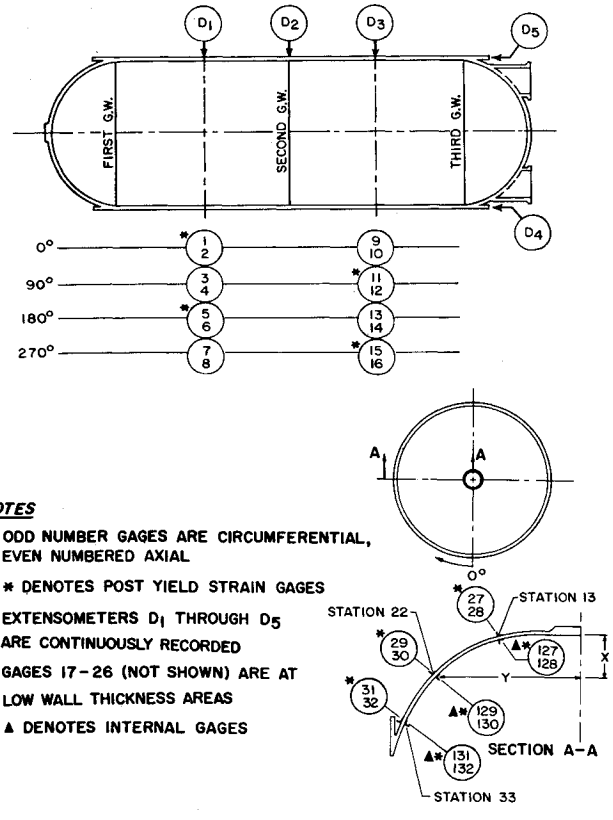

Fig. 3 Typical instrumentation of a 65-in.-diam D6AC rocket motor case.

Based on a biaxial stress field, an equivalent strain (e_i) is determined by substituting the measured principal strains (ϵ_1 and ϵ_2) into Eq. (1), derived from the distortion energy principle. The stress (σ_i) corresponding to (e_i) was obtained from the uniaxial stress-strain curves for the material. In the plastic region, the secant modulus of elasticity (E_s) was taken equal to (σ_i/e_i). The equations used are as follows:

$$e_i = [(1 - \mu + \mu^2)(\epsilon_1^2 + \epsilon_2^2 - \epsilon_1\epsilon_2) + 3\mu\epsilon_1\epsilon_2]^{1/2}/(1 - \mu^2) \quad (1)$$

$$\mu = \{1 - [(1 + \delta)/(1 + e_i)]^{1/2}\}/e_i \quad (2)$$

$$\delta = (1 + \epsilon_{PL})(1 - \mu_{PL}\epsilon_{PL}) - 1 \quad (3)$$

$$\sigma_1 = E_s(\epsilon_1 + \mu\epsilon_2)/(1 - \mu^2) \quad (4)$$

$$\sigma_2 = E_s(\epsilon_2 + \mu\epsilon_1)/(1 - \mu^2) \quad (5)$$

in which

e_i = equivalent strain, in./in.
ϵ_1 = strain in direction of gage 1, in./in.
ϵ_2 = strain in direction of gage 2, in./in.
ϵ_{PL} = proportional limit strain from the uniaxial stress-strain curves of the material, in./in.
μ = Poisson's ratio (dimensionless)
μ_{PL} = elastic range value of Poisson's ratio
δ = const
E_s = secant modulus of elasticity, psi
σ_1 = stress in direction of gage 1, psi
σ_2 = stress in direction of gage 2, psi

In Eq. (1) the Poisson's ratio (μ) is not constant. Since, in Eqs. (1) and (2), the values of μ and e_i are interdependent, an iteration process is necessary to evaluate the proper μ and e_i which will satisfy both equations. Once the value e_i is established, the secant modulus E_s can be evaluated from the uniaxial stress-strain of the material. Using the appropriate μ, E_s, ϵ_1, and ϵ_2, the stresses σ_1 and σ_2 are calculated from Eqs. (4) and (5).

To facilitate the reduction of a large number of strain data, the foregoing analytical procedure was programed on a digital computer. Other methods of reducing strain data in the plastic range have been proposed.[5, 6] However, using the material properties considered in this paper, the maximum stresses computed by the various methods do not differ significantly from each other.

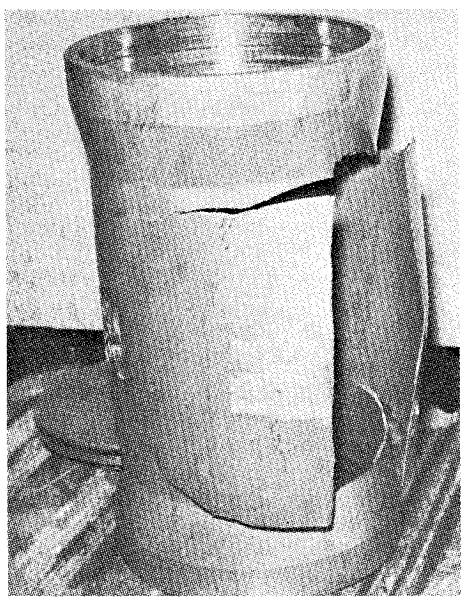

Fig. 4 Typical longitudinal view of a burst 14-in.-diam D6AC subscale vessel.

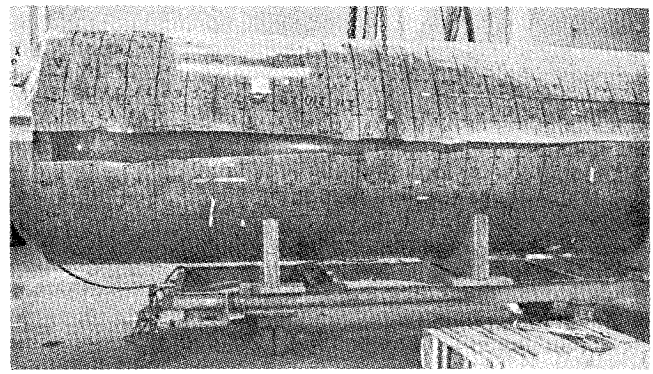

Fig. 5 Longitudinal view of a burst 65-in.-diam D6AC motor case.

Definition of Biaxial Gains

The distortion-energy theory predicts that, in a 2:1 biaxial stress field, the major true stress at any effective logarithmic strain is 1.155 times the uniaxial true stress at the same logarithmic strain.[7] The effective logarithmic strain is

$$\epsilon_e = (2^{1/2}/3)[(\epsilon_1 - \epsilon_2)^2 + (\epsilon_2 - \epsilon_3)^2 + (\epsilon_3 - \epsilon_1)^2]^{1/2} \quad (6)$$

in which ϵ_1, ϵ_2, and ϵ_3 are the principal logarithmic strains such that

$$\epsilon_1 = \log_e(1 + \epsilon_1^*) \quad (7)$$

and ϵ_1^* being the engineering principal strain.

When the biaxial and uniaxial experimental results are compared in accordance with the foregoing theory, equal logarithmic strains should be used. This procedure is illustrated in Fig. 7 and designated as method *A*. Method *B* in Fig. 7 shows another criterion of obtaining the biaxial gains which uses the major principal engineering strains in lieu of the logarithmic strains. Still another method (method *C*, Fig. 7) derives the biaxial gains by using, respectively, the properties from uniaxial and biaxial stress-strain curves based on major principal strains.

A comparison of biaxial gains computed by the foregoing three methods for a typical gage location in a 65-in.-diam D6AC motor case is given in Table 1. From the values listed, the biaxial gains obtained from methods *A* and *B* do not show any appreciable difference. The reasons are 1) for small strains, the difference between the effective strains and the measured circumferential strain is small; and 2) for large strains corresponding to the ultimate strength, the resulting stresses do not vary significantly when the two different strains are used in the computation.

At small strain levels corresponding to proportional limit and yield strength, the biaxial gains computed by method *C*

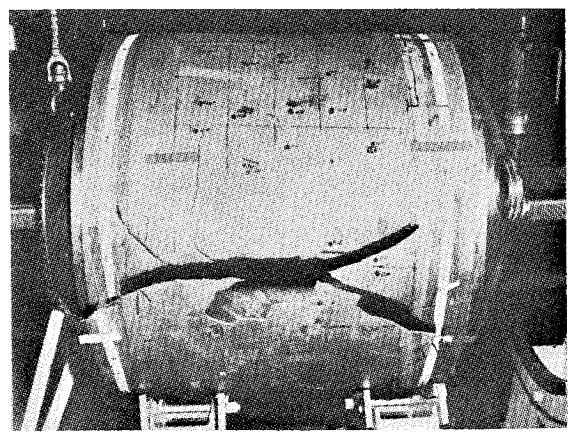

Fig. 6 Close-up of a burst 40-in.-diam 18% Ni motor case.

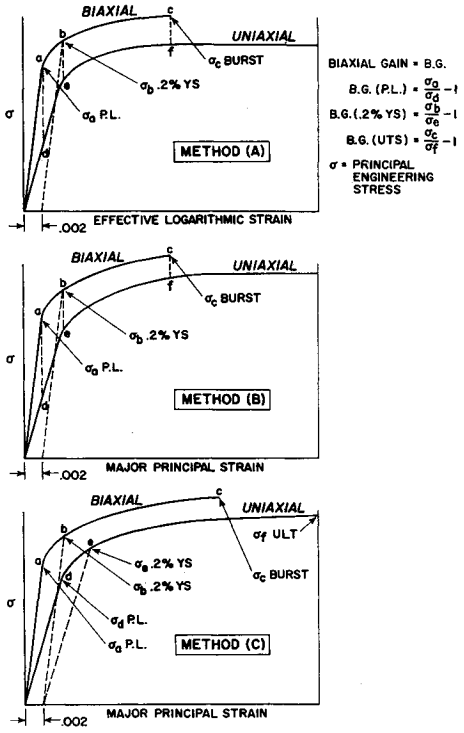

Fig. 7 Methods of computing biaxial gains.

agree well with those by methods *A* and *B*. However, for large strains due to the incompatibility of ultimate strains in the uniaxial and biaxial tests, there is appreciable difference in the biaxial gain values. Since the uniaxial properties for a given material are readily available, method *C*, which relates the biaxial gains with respect to the common engineering uniaxial yield and ultimate strengths, is, for practical purposes, more useful than the other two methods. Hence, in this paper all biaxial gains are computed by using method *C*. In general, for high strength alloy steels with a close proximity between the yield and ultimate strengths, the error introduced by using method *C* is relatively small.

Test Results and Discussions

Using the data-reduction method as described previously, a typical stress-vs-strain diagram from burst-testing of a subscale 14-in.-diam D6AC vessel is obtained in Fig. 8. The strains in the vessel are obtained from gages located in the

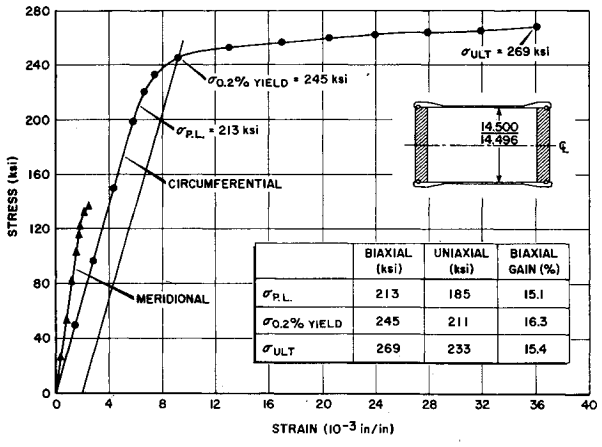

Fig. 8 Typical stress-vs-strain diagram of a burst 14-in.-diam D6AC subscale vessel.

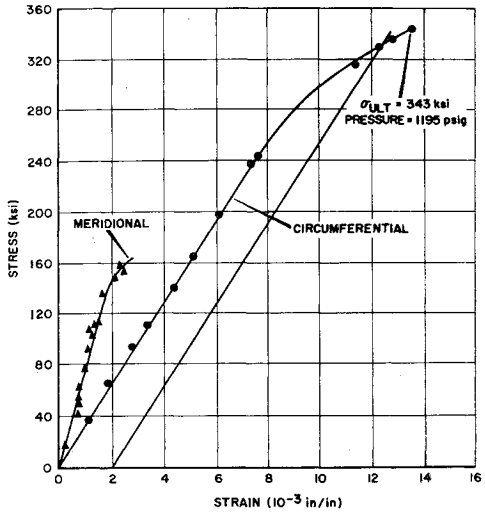

Fig. 9 Stress-vs-strain diagram of a burst 40-in.-diam 18% Ni rocket motor case.

middle section of the cylindrical portion of the vessel. The stresses at the proportional limit, 0.2% yield and the ultimate strengths under the biaxial stressing condition are listed and compared to the uniaxial heat-treated coupon data. Note that the maximum recorded strain in the cylinder at the time of burst is 3.6%.

A similar stress-vs-strain diagram for the 40-in.-diam 18% Ni motor case is given in Fig. 9. The material data from the uniaxial test specimens for various components of the case are given in Table 2. The heat-treat results are obtained from specimens machined from incoming forging cutoff rings and are subsequently heat treated with the actual rocket motor case. From Fig. 9, a maximum biaxial ultimate strength equal to 343 ksi is obtained in the 40-in.-diam 18% Ni case. This strength is approximately 30% higher than those obtained from full-scale D6AC rocket motor cases. The maximum recorded strain in the 18% Ni case is 1.4%. For the 65-in.-diam, 18% Ni motor case, the maximum biaxial ultimate strength obtained was also 343 ksi. A complete comparison of uniaxial and biaxial strengths of Ladish D6AC and 18% Ni maraging steel cases, including full-scale and subscale cases, is given in Table 3.

The biaxial gains for the vessels tested at room temperature as listed in Table 3 are plotted as a function of their respective radius-to-thickness ratios. Figure 10 shows such a plot for gains in 0.2% yield and ultimate strengths. For vessels tested at room temperature, the biaxial gains in yield strength fall in the range of 15.5 to 16.5%. This experimental biaxial gain in the elastic range agrees closely with the Huber-Hencky-Von Mises theory of energy of distortion which predicts that, in a 2:1 biaxial stress field, the major true stress at any effective logarithmic strain is 1.155 times the uniaxial true stress at the same logarithmic strain.

The biaxial gains in the ultimate strengths are found to lie in the range of 13.0 to 16.0%. As mentioned before, these biaxial gains were computed by taking the ratio of the ultimate

Table 1 Comparison of methods *A*, *B*, and *C* for computing biaxial gains

Strength	Biaxial gain, %[a] Method *A*	Method *B*	Method *C*
Proportional limit	16.0	15.0	15.8
0.2% yield	16.0	16.7	16.2
Ultimate strength	15.2	15.0	11.1

[a] See Fig. 7 for graphic representations of methods *A*, *B*, and *C*.

Table 2 Uniaxial heat-treated material data of various components of 40-in.-diam 18% Ni motor case

Strength, ksi		Red. of	Elong.	Hardness
Ult. tensile	0.2% yield	area, %	in 1 in., %	Rockwell C
Aft dome				
302	289	24.3	6.5	54.5
302	289	21.0	5.0	54.5
303	291	23.2	6.0	54.5
Forward dome				
301	294	34.0	8.0	55.0
302	292	30.1	7.0	55.0
301	286	30.4	6.0	55.0
298	286	24.6	6.0	55.0
Centerbody				
292	285	43.0	9.5	53.5
291	277	40.0	8.0	54.5
294	279	40.8	8.0	54.5
293	285	37.7	7.5	55.0

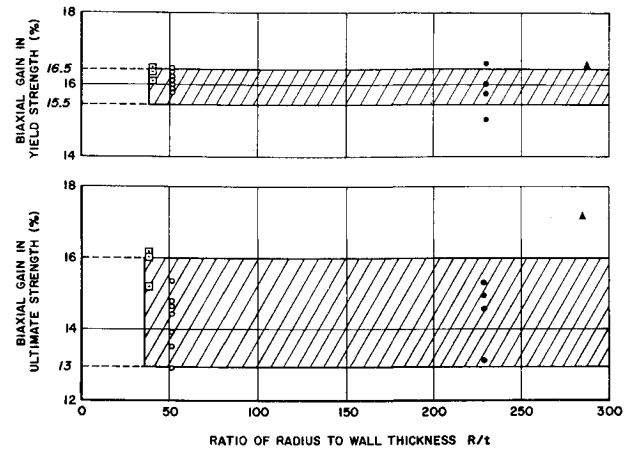

Fig. 10 Percentage biaxial gains vs R/t ratio [for biaxial stress ratio of 2:1 and ratio of cylinder length to diameter (L/D) = 0.7 to 3.2].

strength in the vessel at burst to the uniaxial ultimate coupon strength and then subtracting unity (method *C*, Fig. 7).

For the three subscale tests at elevated temperature of 350°F, the biaxial gains in yield strength are of the same order of magnitude as those in room-temperature tests. However, a significant decrease in biaxial gains in ultimate strength is observed. From Table 3, these gains vary from 9.5 to 10.2%. In obtaining biaxial gains at the elevated temperature, the uniaxial strengths at the same elevated temperature were used.

Figure 10 shows that the biaxial gains in both the yield and ultimate strengths do not vary appreciably in the range of R/t from 40 to 300. Based on same wall thickness, the ratio of diameters of vessels with R/t of 40 and 300 is 1:7.5. Since the cost of bursting large diameter rocket motor cases having R/t of 300 is exceedingly high, the result of this investigation indicates that subscale vessels with a diameter 1/7.5 of the full-scale case will yield reliable results with respect to biaxial gains and the ductility of vessel under biaxial stresses. The length of the subscale vessels should, however, be long enough so that the end restraining effects caused by the closures will not impose bending stresses in the cylinder.

Figure 11 shows comparisons of uniaxial and biaxial stress-vs-strain diagrams for the three D6AC full-scale motor cases

Table 3 Comparison of uniaxial and biaxial strengths

Case designation	Radius, in.	L/D[a]	0.2% yield: Bi-axial, ksi	0.2% yield: Uni-axial, ksi	0.2% yield: Bi-axial gain,[b] %	Ultimate: Bi-axial, ksi	Ultimate: Uni-axial, ksi	Ultimate: Bi axial gain,[b] %	PR/t, ksi	Test temp., °F
a) Full-scale rocket motor cases, Ladish D6AC steel										
65-D6-1	32.75	3.2	225	195	15.0	247	215	15.0	256	Room
65-D6-2	32.75	3.2	236	203	16.0	261	226	15.3	258	Room
65-D6-3	32.75	3.2	255	219	16.7	266	236	13.1	258	Room
b) Subscale vessels, Ladish D6AC steel										
14-D6-1	7.25	1.5	245	211	16.3	269	233	15.4	258	Room
14-D6-2	7.25	1.5	240	206	16.0	258	225	14.5	262	Room
14-D6-3	7.25	1.5	237	204	16.0	252	222	13.5	254	Room
14-D6-4	7.25	1.5	259	223	16.3	264	230	14.7	257	Room
14-D6-5	7.25	1.5	244	210	16.3	264	235	13.0	256	Room
14-D6-6	7.25	1.5	252	216	16.2	274	241	14.0	263	Room
14-D6-7	7.25	1.5	251	216	16.0	276	241	14.5	263	Room
14-D6-8	7.25	1.5	258	223	16.0	268	234	14.8	252	Room
14-D6-9	7.25	1.5	219	219	16.5	265	230	14.5	246	Room
14-D6-10	7.25	1.5	227	195	16.5	248	225	10.2	241	350°
14-D6-11	7.25	1.5	219	186	17.7	242	221	9.5	243	350°
14-D6-12	7.25	1.5	218	186	17.2	243	221	10.0	242	350°
c) Full-scale rocket motor cases 18% Ni maraging steel										
40-18NI-1	20.0	0.7	328	281	16.6	343	292	17.2	345	Room
65-18NI-1	32.75	3.2	337	291	15.8	343	299	14.6	336	Room
d) Subscale vessels 18% Ni maraging steel										
6-18NI-1	3.094	1.5	327	281	16.5	338	291	16.2	345	Room
6-18NI-2	3.094	1.5	326	281	16.2	332	291	15.2	348	Room
6-18NI-3	3.094	1.5	328	281	16.5	338	291	16.0	334	Room

[a] L/D = ratio of length to diameter of cylinder section.
[b] Biaxial gain = biaxial strength/uniaxial strength − 1.

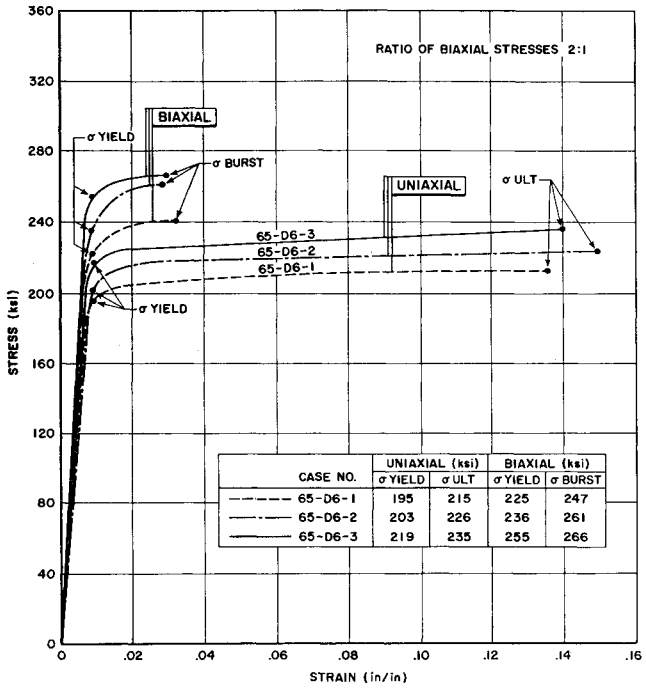

Fig. 11 Comparison of uniaxial and biaxial stress-vs-strain diagrams for three full-scale Ladish D6AC rocket motor cases.

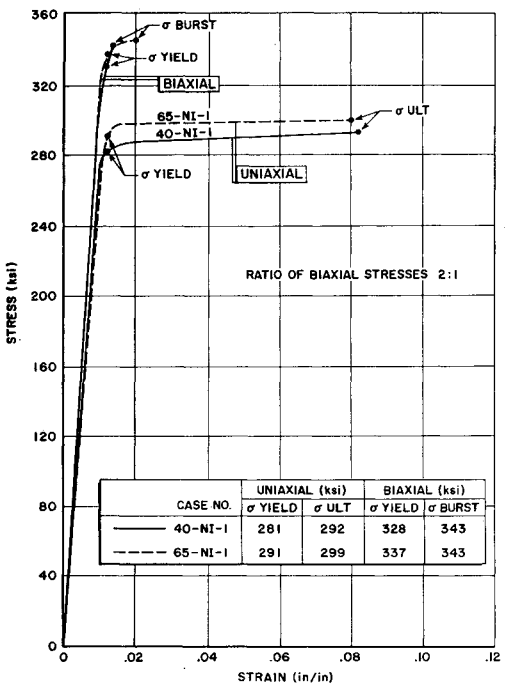

Fig. 12 Comparison of uniaxial and biaxial stress-vs-strain diagrams for two full-scale 18% Ni rocket motor cases.

The biaxial gains in the yield and ultimate strengths are apparent from the curves. One interesting phenomenon observed from these curves is the significant reduction of ductility in the biaxially stressed cylinder as compared to that obtained in the uniaxial specimen. Whereas the elongations of the uniaxial specimens are in the range of 14 to 15%, the maximum elongation at the burst of the vessels is only 3.2%. This apparent decrease of ductility of a metal tested under biaxial stresses has been discussed qualitatively by Ludwik.[1]

Similar comparisons of the uniaxial and biaxial stress-vs strain-diagrams for the 18% Ni motor cases are given in Fig. 12. Here the reduction of the ductility is also pronounced as the elongations are reduced from the uniaxial values of 8.2 and 8.0% to biaxial values of 1.4 and 2.0%, respectively.

In order to achieve lightweight design of large diameter rocket motor cases, the present trend is to use the biaxial strength as a basis of design criteria. Because of the significant loss of the ductility in the biaxial stress field, a structure designed on the basis of a 0.2% biaxial yield strength cannot give the same degree of safety against fracture as the one based on the uniaxial 0.2% yield strength. As seen from Fig. 12, the biaxial 0.2% yield strength is strain-wise a very small distance from the fracture.

It is proposed therefore that, for materials such as the D6AC, a biaxial strength with a 0.05% offset be used as a reference strength criterion. Rocket motor cases using ultra-high strength steels such as 18% Ni steel should be designed based on a biaxial proportional limit strength. Because of the loss of ductility in the biaxial stress field, material discrepancies such as flaws, local embrittlement, and porosities will be more critical in causing premature failures in a vessel than in a uniaxial specimen.

Conclusions

The following conclusions can be made from the results of this investigation:

1) A biaxial ultimate strength equal to 343 ksi has been obtained from burst-testings of two full-size rocket motor cases made of 18% Ni maraging steel. This strength is approximately 30% higher than that of the present "state-of-the-art" D6AC steel.

2) Within the range of radius-to-thickness ratios between 40 and 300, the subscale vessels behave essentially the same as the full-scale rocket motor cases with respect to the biaxial gains and the total elongation of the vessel at failure.

3) In a 2:1 stress field, the experimental biaxial gains in the elastic range are found to vary from 15.5 to 16.5%. This is in close agreement with values predicted by Huber-Hencky-Von Mises theory of constant energy of distortion.

4) The experimental biaxial gains in a 2:1 stress field at vessel fracture are found in the range of 13 to 16%.

5) The total elongations in the cylindrical vessels at failure are approximately one-fifth of those obtained from the uniaxial specimens.

References

[1] Nadai, A., *Theory of Flow and Fracture of Solids* (McGraw-Hill Book Co., Inc., New York, 1963), pp. 209–210, 250–251.

[2] Wei, B. C. F., "Structural analysis of solid propellant rocket casings," ARS Preprint 1590–61 (February 1961).

[3] Wei, B. C. F. and Nielsen, P., "A computer analysis of large booster structures for design optimization," Society of Automotive Engineers Paper 746A (September 1963).

[4] Ades, C. S., "Reduction of strain rosettes in the plastic range," J. Aerospace Sci. **26**, 392–393 (1959).

[5] Pian, T. H. H., "Reduction of strain rosettes in the plastic range," J. Aerospace Sci. **26**, 842–843 (1959).

[6] Ades, C. S., "Reduction of strain rosettes in the plastic range," Society of Experimental Stress Analysis Paper 733 (May 1962).

[7] Sachs, G., Schapiro, L., and Hoffman, O., "Strength of ductile metal motor cases," ARS Preprint 2419–62 (April 1962).